DRAFT VERSION APRIL 10, 2013
Preprint typeset using LaTeX style emulateapj v. 5/2/11

arXiv:1304.2633v1 [astro-ph.HE] 9 Apr 2013

# A REFLECTION MODEL FOR THE CYCLOTRON LINES IN THE SPECTRA OF X-RAY PULSARS

JURI POUTANEN[1], ALEXANDER A. MUSHTUKOV[1,2,3], VALERY F. SULEIMANOV[4,5], SERGEY S. TSYGANKOV[6,1,7],
DMITRIJ I. NAGIRNER[2], VICTOR DOROSHENKO[4], AND ALEXANDER A. LUTOVINOV[7]
[1] Astronomy Division, Department of Physics, PO Box 3000, FI-90014 University of Oulu, Finland; juri.poutanen@oulu.fi
[2] Sobolev Astronomical Institute, Saint Petersburg State University, Saint-Petersburg 198504, Russia
[3] Pulkovo Observatory of Russian Academy of Sciences, Saint-Petersburg 196140, Russia
[4] Institut für Astronomie und Astrophysik, Kepler Center for Astro and Particle Physics, Universität Tübingen, Sand 1, 72076 Tübingen, Germany
[5] Kazan (Volga region) Federal University, Kremlevskaja str., 18, Kazan 420008, Russia
[6] Finnish Centre for Astronomy with ESO (FINCA), University of Turku, Väisäläntie 20, FI-21500 Piikkiö, Finland
[7] Space Research Institute of the Russian Academy of Sciences, Profsoyuznaya Str. 84/32, Moscow 117997, Russia

*Draft version April 10, 2013*

## ABSTRACT

Cyclotron resonance scattering features observed in the spectra of some X-ray pulsars show a significant changes of the line energy with the pulsar luminosity. At high luminosities, these variations are often associated with the onset and growth of the accretion column, which is believed to be the origin of the observed emission and of the cyclotron lines. However, this scenario inevitably implies large gradient of the magnetic field strength within the line-forming region, which makes the formation of the observed line-like features problematic. Moreover, the observed variation of the cyclotron line energy is much smaller than could be anticipated for the corresponding luminosity changes. We argue here that a more physically realistic situation is that the cyclotron line forms when the radiation emitted by the accretion column is reflected from the neutron star surface, where the gradient of the magnetic field strength is significantly smaller. We develop here the reflection model and apply it to explain the observed variations of the cyclotron line energy in a bright X-ray pulsar V 0332+53 over a wide range of luminosities.

*Subject headings:* line: formation – pulsars: general – relativistic processes – scattering – stars: neutron – X-rays: binaries

## 1. INTRODUCTION

X-ray pulsars are neutron stars in binary systems accreting matter usually from a massive companion. These neutron stars have a sufficiently strong magnetic field, which channels accreting gas towards magnetic poles. Strong magnetic field modifies the observed X-ray spectrum often manifesting as the line-like absorption features, the so-called cyclotron lines. Such cyclotron resonance scattering features (CRSF), sometimes also with harmonics, are observed in the spectra of several X-ray pulsars (Coburn et al. 2002; Filippova et al. 2005; Caballero & Wilms 2012).

In some cases, the luminosity related changes of the line energy are observed, suggesting that configuration of the line-forming region depends on the accretion rate. The line energy has been reported to be positively (in relatively low-luminosity sources; see Staubert et al. 2007; Klochkov et al. 2012) and negatively-correlated with luminosity (in high-luminosity sources; see Mihara et al. 1998; Tsygankov et al. 2006), as well as uncorrelated with it (Caballero et al. 2013).

This diversity is yet to be explained, and in this work we will focus only on the high-luminosity case. The negative correlation of the CRSF energy with luminosity here is usually explained with the onset and growth of the accretion column at high luminosities (Basko & Sunyaev 1976). In this scenario, the height of the column, and, therefore, the average displacement of the emission and the line-forming regions from the neutron star surface increase with luminosity. The magnetic field weakens rapidly with distance from the neutron star and, therefore, the CRSF should shift to lower energies. The problem is, however, that the predicted shift is much larger than the observed one. The column height depends on luminosity almost linearly (Basko & Sunyaev 1976) and the magnetic field weakens with distance as $r^{-3}$, and yet brightening by more than an order of magnitude yields at most 25% decrease in the CRSF energy (Tsygankov et al. 2006, 2010). Moreover, large gradient of the magnetic field and of the accretion velocity are expected to smear out the line-like features making it difficult to explain why we observe CRSFs at all.

Several authors (Burderi et al. 2000; Kreykenbohm et al. 2008) considered variation of the magnetic field along the neutron star surface as a possibility to explain the observed variation of the cyclotron line energy with the pulse phase, which has similar magnitude as those associated with the luminosity changes. Interaction of accreting plasma with the magnetosphere of the neutron star defines the geometry of the emission region, so one could imagine that a change in the accretion rate could also offset the location of the polar cap, leading to a change in the observed CRSF energy. However, the observed variations would imply an unrealistically large shift of the hotspot location (by 50–60 degrees) from the magnetic pole. Furthermore, the observed change in the CRSF energy in this case would imply a dramatic change in the pulse profile shape, which is not observed.

On the other hand, a significant part of the column radiation should be intercepted by the stellar surface because of the relativistic beaming (Kaminker et al. 1976; Lyubarskii & Sunyaev 1988). Small variations of the $B$-field strength over the surface (only by a factor of two in the case of the dipole field) would imply that the variations of the typical cyclotron energy are small. Thus, it is more natural to assume that the line is formed in the atmosphere of the neutron star due to reflection of the intercepted radiation. Increase in the mass accretion rate results in a larger luminosity, a higher column height and a larger illuminated part of the stellar surface (see Fig. 1). If the $B$-field decreases away from the magnetic

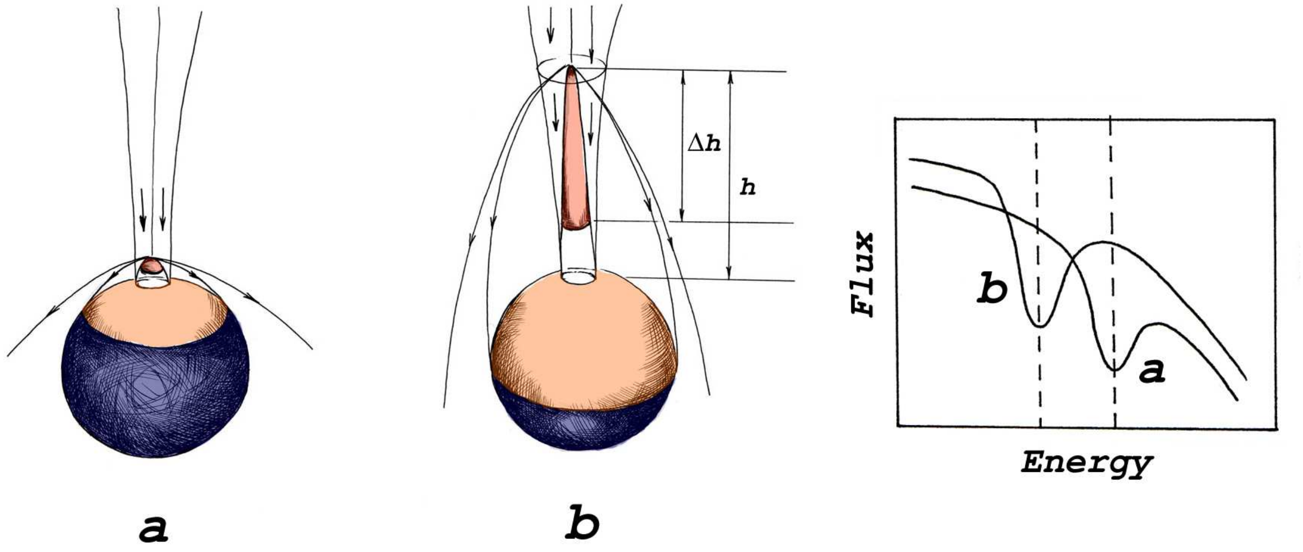

**Figure 1.** Sketch of the accreting X-ray pulsar geometry and the emergent spectrum. The larger is the accretion rate, the higher is the column, the larger illuminated fraction of the stellar surface, the weaker the average magnetic field, and the smaller the cyclotron line energy.

poles, the cyclotron line energy should then decrease with the luminosity and a negative correlation between the luminosity and the cyclotron line energy is reproduced. Here we discuss this scenario quantitatively and compare the model predictions with the data taking during a bright outburst of the transient X-ray pulsar V 0332+53.

## 2. MODEL SET UP

Let us start from the physical picture of the accretion on the magnetized neutron star following earlier papers by Basko & Sunyaev (1976) and Kaminker et al. (1976). It is possible to distinguish the two regimes of accretion onto magnetized neutron stars depending on the mass accretion rates. At low accretion rate, free-falling protons heat part of the neutron star surface near its magnetic poles, and these bright spots radiate energy in the X-ray range. At high accretion rate, radiation pressure becomes significant and stops the infalling material above the neutron star surface in the radiation-dominated shock. Below the shock, the matter slowly sinks down as the excess emission supporting the column escapes through the side walls. The column is expected to arise as soon as the luminosity exceeds a critical value (Basko & Sunyaev 1976):

$$L^* \approx 4\times 10^{36} \left(\frac{\kappa_{\rm T}}{\kappa_{\|}}\right) \left(\frac{5l}{R}\right) \left(\frac{M}{M_{\odot}}\right)\ {\rm erg\ s^{-1}}, \qquad (1)$$

where $\kappa_{\|}$ is the electron scattering opacity along the magnetic field, $\kappa_{\rm T}$ is the Thomson opacity, $M$ and $R$ are the mass and the radius of the star, $l$ is the length of the accretion arc at the stellar surface. It is worth noticing that the optical depth across the column is of the order $L/L^*$ and $L^*$ is much larger than the Eddington luminosity scaled to the area of the footprint of the accretion column and depends on the accretion flow geometry.

The column height depends on the accretion rate (Basko & Sunyaev 1976; Lyubarskii & Sunyaev 1988):

$$\frac{h}{R} = \dot{m}\ \ln\left(\eta\frac{1+\dot{m}}{\dot{m}^{5/4}}\right), \qquad (2)$$

where

$$\begin{aligned}\eta &= \left(\frac{B^2 d^2 \kappa_{\|}}{7\pi c\sqrt{2GMR}}\right)^{1/4} \\ &= 16\left(\frac{B}{5\times 10^{12}\ {\rm G}}\right)^{1/2} \left(\frac{d}{100\ {\rm m}}\right)^{1/2} \left(\frac{\kappa_{\|}}{0.4}\right)^{1/4}, \qquad (3)\end{aligned}$$

$d$ is the thickness of the accretion arc, and $\dot{m} = L/L^{**}$ is a ratio of the X-ray pulsar luminosity to the limiting luminosity for the magnetized neutron star

$$L^{**} \approx 10^{39} \left(\frac{l/d}{50}\right) \left(\frac{\kappa_{\rm T}}{\kappa_{\|}}\right) \left(\frac{M}{M_{\odot}}\right)\ {\rm erg\ s^{-1}}, \qquad (4)$$

which corresponds to the column height of $h \gtrsim R$. The height, where matter stops, varies inside the accretion channel and depends on the distance from its borders because the radiation energy density drops off sharply towards the edge of the column. The height has its maximum value near the middle of the channel and decreases towards the borders. Therefore, the radiation from the already stopped matter should pass through a layer of the rapidly falling plasma. These outer layers of the column are not supported by the radiation and fall with velocity close to the free-fall velocity $\beta = v/c = \sqrt{r_{\rm S}/r}$ (here $r_{\rm S} = 2GM/c^2$ is the Schwarzschild radius). The optical thickness of these layers is high enough to change significantly the angular distribution of the emergent radiation. As a result, the radiation is directed mainly towards the stellar surface due to the relativistic beaming. For the electron-scattering dominated column, the angular distribution of the column luminosity in the laboratory frame is given by (see Appendix A and Kaminker et al. 1976; Mitrofanov & Tsygan 1978):

$$\frac{dL(\alpha)}{d\cos\alpha} = I_0\ \frac{D^4}{\gamma} 2\sin\alpha \left(1+\frac{\pi}{2}D\sin\alpha\right), \qquad (5)$$

where $\alpha$ is the angle between the photon momentum and the velocity vector, $\gamma = 1/\sqrt{1-\beta^2}$ is the Lorentz factor, $D = 1/[\gamma(1-\beta\cos\alpha)]$ is the Doppler factor, and $I_0$ is the

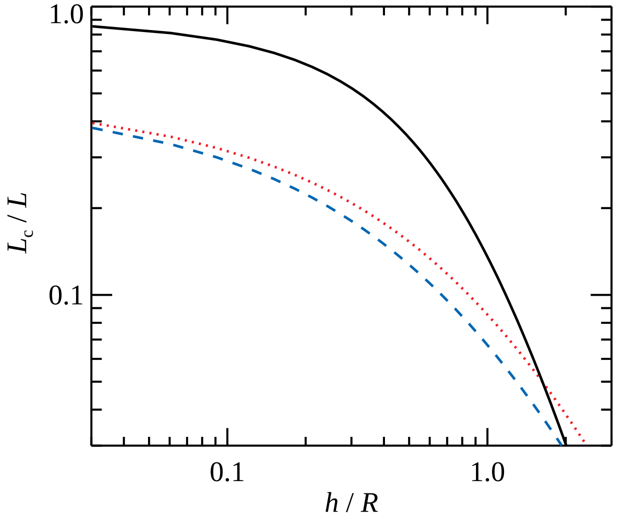

**Figure 2.** Fraction of the captured radiation from a point source above the neutron star surface as a function of the height-to-radius ratio. The dashed blue curve corresponds to the isotropic source in flat space-time, the dotted red curve is for the isotropic source accounting for light bending in Schwarzschild metric, and the solid black curve is for the emission pattern given by equation (5) and accounting for light bending. Here $R = 3r_{\mathrm{S}}$.

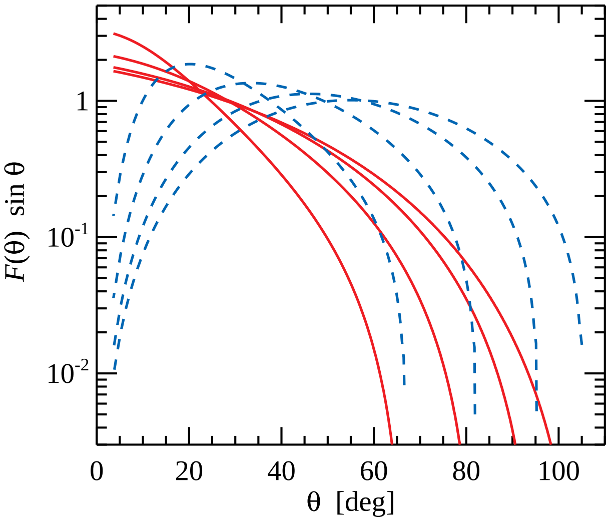

**Figure 3.** Dependence of the normalized flux on co-latitude for an accretion column emitting according to the law (5) with constant luminosity per unit height (i.e. constant $I_0$). The flux is normalized as $\int F(\theta)\sin\theta d\theta = 1$. The red solid lines correspond to $\Delta h/h = 1$ and the blue dashed lines to $\Delta h/h = 0$. Different lines show the distribution for various column heights: $h/R = 0.5, 1, 2$ and $4$ (from left to right). Here $R = 3r_{\mathrm{S}}$.

normalization constant. The emission pattern becomes more isotropic at large $r$, because of the radial dependence of the free-fall velocity.

The energy release and the distribution of the emerging radiation flux along the accretion column depends on the details of radiation–matter interaction and is a complicated radiation-hydrodynamical problem. For simplicity, we approximate the geometry of the accretion column by a thin stick on the magnetic pole. This approximation is reasonably accurate for high $B$-field pulsars up to $h \lesssim R$. Here we also assume that most energy is emitted in a region of characteristic scale $\Delta h$ situated above the neutron star surface at height $h$ (see Fig. 1), so $\Delta h/h = 1$ for a homogeneously emitting column, or $\Delta h/h = 0$ if all the energy is emitted within a thin shock at the top of the column.

Results weakly depend on the compactness of the star, which we fix here at $R/r_{\mathrm{S}} = 3$ (corresponding to the radius of 13 km for a $1.5M_{\odot}$ neutron star, consistent with the recent measurements from X-ray bursters, see e.g. Suleimanov et al. 2011).

## 3. REFLECTED FRACTION AND SURFACE FLUX DISTRIBUTION

At a high accretion rate, the accretion column radiates the released gravitational energy of the falling matter through its sides. Part of the radiation leaves the system directly and part of it is captured by the stellar surface. The fraction of the captured radiation $L_{\mathrm{c}}/L$ depends on the height of the column, brightness distribution over the column, radiation beam pattern and the compactness of the star. In Schwarzschild metric, for an isotropic, point-like source at radius $r$, it is given by a simple formula (see Appendix B):

$$\frac{L_{\mathrm{c}}(r)}{L} = \frac{1}{2}\left(1 - \cos\alpha_{\max}\right), \tag{6}$$

with

$$\sin\alpha_{\max} = \frac{R}{r}\sqrt{\frac{1 - r_{\mathrm{S}}/r}{1 - r_{\mathrm{S}}/R}}. \tag{7}$$

In case of flat space-time, we can substitute $r_{\mathrm{S}} = 0$. The captured fraction is slightly higher when light bending is accounted for. It drops from the maximal value of 0.5 to 0.1 when the source rises to $h \sim R$ (see Fig. 2).

For the emission pattern given by equation (5) and used in the following calculations, the captured fraction increases even further, because of the strong beaming towards the star (see top curve in Fig. 2). For a higher source position, $L_{\mathrm{c}}/L$ drops below the isotropic case at $h \sim 2R$, because of a rather small beaming resulting from a smaller free-fall velocity and a factor $\sin\alpha$, which reduces the radiation directed along the column.

Variations in the emission height lead also to a dramatic change in the distribution of the captured flux $F(\theta)$ over the stellar surface. We illustrate this effect here by considering a homogeneously emitting column (i.e. $I_0 =$ const in equation 5) of various heights and $\Delta h/h$ (see Fig. 3). The details of the calculations can be found in Appendix B. For a low column, most of the emission hits the surface in the direct vicinity of the column at a co-latitude $\theta \lesssim \sqrt{2h/R}$ and the flux drops rapidly with distance from the column. For $\Delta h/h = 1$, the flux $F(\theta)$ diverges as $1/\theta$, which is a consequence of our assumption of an infinitely thin column. When $h \approx R$, the star is irradiated almost up to the equator and for even higher column, most of the stellar surface receives some flux. In a realistic pulsar, the captured flux is a sum of the contribution from the two antipodal columns.

## 4. FORMATION OF THE CYCLOTRON LINE

Radiation from the accretion column hits the neutron star surface and is reflected. The most important process affecting the spectrum of the reflected radiation is Compton scattering. Under the conditions of the neutron star atmosphere, the density is too small to produce any true absorption of the hard X-ray photons either in the continuum or at the cyclotron line energy. The cross-section for Compton scattering in strong magnetic field is energy-dependent and has strong resonances at

$$\frac{E_{\rm res}^{(n)}(B)}{m_{\rm e}c^2} = \begin{cases} \dfrac{\sqrt{1+2nb\sin^2\xi}-1}{\sin^2\xi}, & \text{for } \xi \neq 0, \quad n=1,2,..., \\ b, & \text{for } \xi = 0, \end{cases} \tag{8}$$

where $b \equiv B/B_{\rm cr}$ is the $B$-field strength in units of the critical field strength $B_{\rm cr} = m_{\rm e}^2 c^3/e\hbar = 4.412 \times 10^{13}$ G, $\xi$ is the angle between the field and photon momentum, and $m_{\rm e}$ is the electron mass. For $b \ll 1$, the resonance energies are $E_{\rm res}^{(n)}/m_{\rm e}c^2 \approx bn$.

Photons at the resonance energies cannot penetrate deep into the atmosphere, they interact in the surface layers and scatter back. In the cyclotron line wings, photons penetrate deeper into the atmosphere and scatter there with some energy shift. If they scatter into the resonance energy, they cannot leave the atmosphere because of the larger optical depth there and escape instead in the line wings. Thus, the lack of the photons near the resonance is not filled in. The absorption feature at the resonance energy and the emission features in the wings appear in the spectrum of the reflected radiation. The energy separation between the emission peaks can reach many Doppler widths (see Avrett 1965, Avrett & Hummer 1965, and Sect. 6.4 of Ivanov 1973). Because the emission lines are broad, they merge with the continuum and cannot be easily separated. For resonant Compton scattering in magnetic field, the line is not symmetric and the red wing of the emission line is stronger, because of the recoil (Wasserman & Salpeter 1980; Araya & Harding 1999; Araya-Góchez & Harding 2000; Harding & Lai 2006), which gives the relative photon energy shift of about $\Delta E/E \sim -E_{\rm res}/m_{\rm e}c^2 \approx -b$. The absorption features at the harmonic energies can be even stronger, because the absorbed photons are mostly reemitted at the energy of the fundamental. The typical X-ray pulsar spectrum cuts off at ∼30–50 keV and therefore the contribution of the harmonics will be negligible in high-field pulsars (as is the case of V 0332+53).

Neglecting the asymmetry in the line shape, the centroid of the CRSF in the reflected spectrum averaged over the surface and all angles is determined by the $B$-field strength weighted with the distribution of flux, $F(\theta)$ (Fig. 3), and the line equivalent width, EW$(\theta)$, over the neutron star surface:

$$E_{\rm cycl} = \frac{m_{\rm e}c^2}{1+z} \frac{\int_0^\pi b(\theta)F(\theta)\ {\rm EW}(\theta)\ \sin\theta\ d\theta}{\int_0^\pi F(\theta)\ {\rm EW}(\theta)\ \sin\theta\ d\theta}, \tag{9}$$

where $z$ is the gravitational redshift. Assuming that the line EW in the reflected radiation is constant over the surface, we can relate the cyclotron line centroid to the mean field as

$$E_{\rm cycl} = \frac{m_{\rm e}c^2}{1+z}\frac{\langle B\rangle}{B_{\rm cr}}, \tag{10}$$

where

$$\langle B\rangle = \frac{\int_0^\pi B(\theta)F(\theta)\sin\theta\ d\theta}{\int_0^\pi F(\theta)\sin\theta\ d\theta}. \tag{11}$$

Variations of the magnetic field over the surface lead to the smearing of the line and its minimum width is then related to the magnetic field standard deviation:

$$\sigma_B = \frac{\int_0^\pi \left[B(\theta)-\langle B\rangle\right]^2 F(\theta)\sin\theta\ d\theta}{\int_0^\pi F(\theta)\sin\theta\ d\theta}. \tag{12}$$

If $(\sigma_B/\langle B\rangle)\times E_{\rm cycl}$ is smaller or comparable to the separation between the emission peaks, the CRSF will remain strong in the total spectrum of the reflected radiation.

At low accretion rate, the column is very low, $h/R \ll 1$, and only the polar region is illuminated, resulting in the line energy $E_{\rm cycl} = E_0$ corresponding to the polar field $B_0$. Because for the dipole field, the $B$-field strength drops only by a factor of two from the pole to the equator, there is an obvious limitation for changes in the cyclotron line energy: the line should lie in the energy interval $[E_0/2; E_0]$. A more realistic lower limit on the line energy can be obtained assuming a uniformly illuminated surface, i.e. $F(\theta) = {\rm const}$. In that case

$$\langle B\rangle_{\rm min} = \frac{1}{4}B_0 \int_0^\pi \sin\theta\sqrt{1+3\cos^2\theta}\ d\theta \simeq 0.7B_0. \tag{13}$$

Therefore, the line should not change its energy significantly and the model predicts the range for the line centroids of $[0.7E_0; E_0]$ in agreement with observations (Tsygankov et al. 2006, 2010).

In Fig. 4, we present theoretical dependences of the mean magnetic field, standard deviation, and the captured fraction on the height of the column for different values of $\Delta h/h$. These quantities will have a similar behavior as a function of luminosity too. We see that for the point-like source, variations in all quantities are the largest, while for a homogeneously emitting column, they are the smallest. If the whole column emits (i.e. $\Delta h/h = 1$), the polar regions are always strongly illuminated and $\langle B\rangle$ varies by only 10%. On the other hand, for $\Delta h/h = 0$, the mean field varies by at least 25%. A negative correlation between the column height (luminosity) and the cyclotron line energy is produced. The smearing of the line, because of the magnetic field variation, does not reach more that 10–15% (see Fig. 4b). Thus if the emission peaks in the reflected radiation are separated by more than 20%, the CRSF would remain strong even at high $h/R$. The strength of the CRSF in the total spectrum depends also linearly on the captured luminosity fraction and is expected to decrease at high column (see Fig. 4c); therefore, a correlation between the line equivalent width and the energy is expected.

## 5. COMPARISON WITH OBSERVATIONS

We would like to compare our model with the data from the X-ray pulsar V 0332+53 obtained with the *RXTE* and *INTEGRAL* observatories during outburst in 2004–2005 (Tsygankov et al. 2006, 2010). This source shows negative correlation between the luminosity and the energy of the cyclotron line. It is the only data set which has the information about the behavior of the object in a so wide range of the luminosities, from $\sim 10^{37}$ up to $\sim 4\times10^{38}$ erg s$^{-1}$.

For a given parameter of the accretion column $\Delta h/h$, we compute the distribution of the reflected flux $F(\theta)$ as a function of the column height $h$. This is then converted to the average magnetic field $\langle B\rangle$ in units of the polar one $B_0$ us-

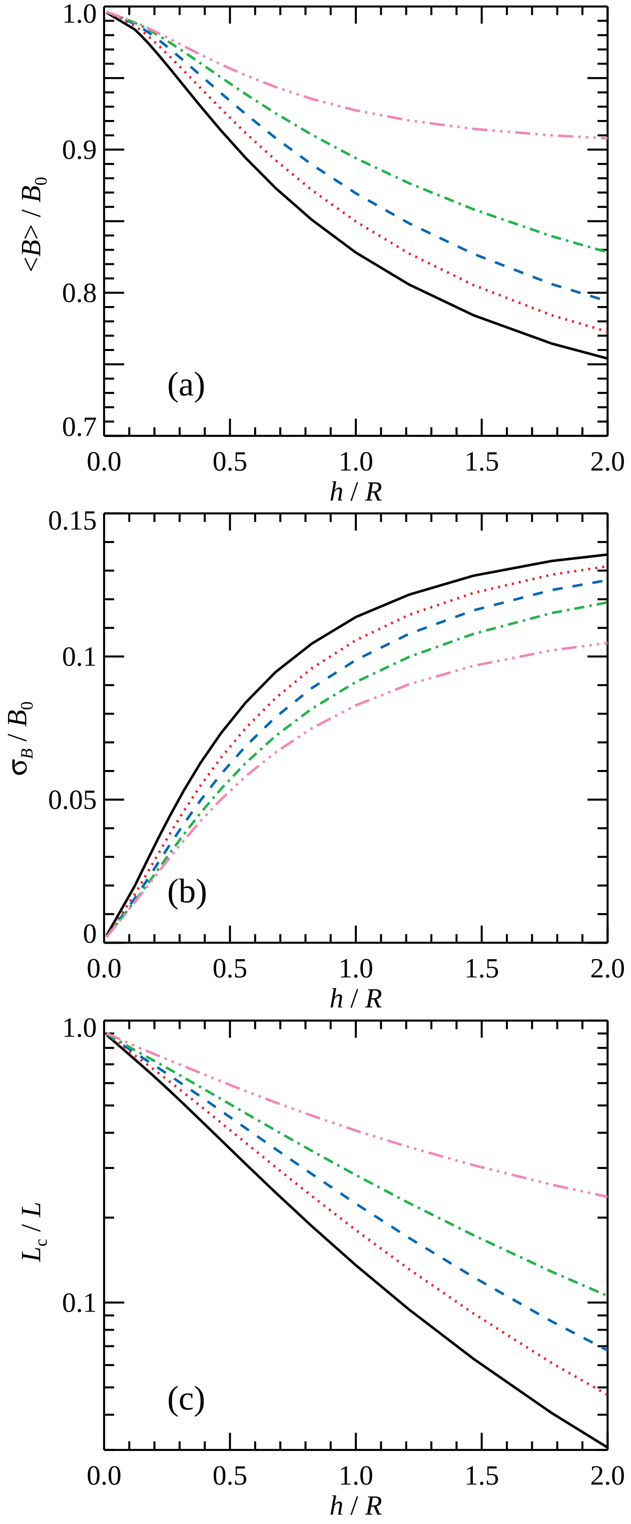

**Figure 4.** Theoretical dependences of (a) the mean magnetic field in the reflecting zone for dipole field (in units of polar field) as defined by equation (11), (b) the magnetic field standard deviation given by equation (12), and (c) the fraction of the captured luminosity on the $h/R$ ratio for $R = 3r_{\rm S}$. Black solid, red dotted, blue dashed, green dot-dashed and pink triple-dot-dashed line correspond to $\Delta h/h$=0, 0.3, 0.5, 0.7, 1.0, respectively.

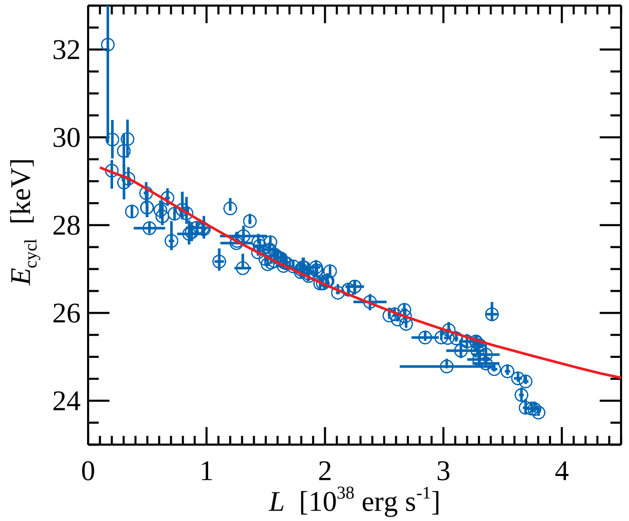

**Figure 5.** Dependence of the cyclotron line energy on the luminosity in the X-ray pulsar V 0332+53 (circles with the error bars; from Tsygankov et al. 2010) and the best-fit theoretical relation (solid line) for $\Delta h/h = 0.1$, $\eta = 15$, $E_0 = 29.5$ keV, and $L^{**} = 21 \times 10^{38}$ erg s$^{-1}$.

**Table 1**
Best-fit parameters

| $\Delta h/h$ | $E_0$ (keV) | $L^{**}$ ($10^{38}$ erg s$^{-1}$) | $\chi^{2}$ [a] |
|---|---|---|---|
| 0.0 | 29.5±0.2 | $22.3^{+2.4}_{-1.7}$ | 96.4 |
| 0.1 | 29.5±0.2 | 20.9±1.8 | 96.4 |
| 0.2 | 29.5±0.2 | $19.4^{+1.9}_{-1.5}$ | 97.3 |
| 0.3 | 29.6±0.2 | 17.8±1.6 | 98.5 |
| 0.4 | 29.6±0.2 | 16.1±1.6 | 100.0 |
| 0.5 | 29.6±0.2 | 14.3±1.6 | 103.7 |
| 0.6 | 29.6±0.3 | $12.4^{+1.4}_{-1.8}$ | 108.4 |
| 0.7 | $29.7^{+0.5}_{-0.3}$ | $10.2^{+1.6}_{-2.0}$ | 116.7 |
| 0.8 | $29.9^{+1.0}_{-0.3}$ | $7.6^{+1.1}_{-3.2}$ | 130.6 |
| 0.9 | $32.8^{+0.3}_{-0.7}$ | $1.1^{+0.35}_{-0.13}$ | 124.2 |
| 1.0 | $28.7^{+0.3}_{-0.3}$ | $12.5^{+2.4}_{-2.8}$ | 227.3 |

[a] For 94 degrees of freedom.

ing equation (11) assuming a dipole field and to the cyclotron line energy $E_{\rm cycl}$ in units of the polar value $E_0$ using equation (10). Transition from the dependence on $h$ to the dependence on the luminosity is made as discussed in Sect. 2 using equation (2), where $\eta$ and $L^{**}$ are the parameters.

The cyclotron-line energy dependence on the luminosity for the X-ray pulsar V 0332+53 (Tsygankov et al. 2010) is shown in Fig. 5. It is clear that the data at luminosities above $3.6 \times 10^{38}$ erg s$^{-1}$ cannot be described by our model and we neglect them in the fits. The remaining data are fitted with two free parameters $E_0$ and $L^{**}$. We fix $\eta = 15$ (see equation 3), because the results depend on that parameter very weakly and vary $\Delta h/h$ in the range between 0 and 1 with the step 0.1. Taking the errors on measured $E_{\rm cycl}$ at their face values, gives the reduced $\chi^2$ significantly above unity, because of a large spread of the line energies at a fixed luminosity. Therefore, we add a systematic error of 0.15 keV in quadrature to the statistical errors of $E_{\rm cycl}$. A good agreement with the data, with the $\chi^2$ values below 100 (for 94 degrees of freedom), is achieved for $E_0 \approx 29.5$ keV, $\Delta h/h \lesssim 0.4$ and $L^{**} \approx 2 \times 10^{39}$ erg s$^{-1}$ (see Table 1). The $\chi^2$ grows with $\Delta h/h$ and $L^{**}$ decreases from about $2.2 \times 10^{39}$ erg s$^{-1}$ to $10^{39}$ erg s$^{-1}$ when $\Delta h/h$

changes from 0 to 0.7. The values of $L^{**}$ obtained in the fits should be taken as the upper limits on the actual value given by equation (4), because the radiation from the upper part of the column might be completely blocked by the falling material and photons escape only at a height significantly smaller than the top of the accretion shock.

The fitting procedure seems to indicate that the best description of the data is achieved for a column with most of the emission coming from its top. This does not necessarily mean that the lower part is not emitting, but rather that this emission does not hit the neutron star surface. It is actually expected, because in the lower part of the column the optical depth of the falling plasma above the shock becomes smaller and the photons from the shock freely escape to the observer. Furthermore, our results are based on the assumption of the constant with latitude equivalent width. In reality, the scattering opacity is a strong function of the angle between the photon momentum and the magnetic field (see e.g. Pavlov et al. 1980; Suleimanov et al. 2012), which necessarily will result in some latitude dependence and possibly will increase the line EW of the spectrum reflected from the equatorial region. In that case, our result of the top-dominated emission from the column might be an artifact of this effect.

The best-fit parameter indicate that the height of the column reaches $R$ at $L \sim 4 \times 10^{38}\ \mathrm{erg\,s^{-1}}$. This is close to the luminosity, where large deviations of the model from the data are visible. The possible reason for this mismatch is that our approximation of the accretion column by a thin stick breaks down. In addition, at such large $L$, radiation from the high anti-podal column starts to hit the equatorial region and becomes observable. This reduces the average "observed" $B$-field. In our model, the presented quantities are averaged over all observer angles and this effect is not accounted for.

## 6. SUMMARY

In this paper, we have proposed a reflection model for the cyclotron line formation in X-ray pulsars. At high accretion rates, the accretion column is predicted to have a significant height illuminating a large fraction of the neutron star surface. Strong beaming of the column radiation towards the surface guaranties that a significant fraction of the column emission is reflected from the surface.

We argued that the reflected spectrum should have a strong CRSF at the energy depending on the local magnetic field strength. Small variations of the magnetic field along the surface imply that the line centroid energy can vary by at most 30%, from the value corresponding to the field at the pole to the whole surface-averaged field. Changes in the pulsar luminosity are expected to correlate with the illuminated fraction of the stellar surface, and anti-correlate with the average magnetic field and, therefore, with the line centroid energy, exactly as observed during the outburst of the X-ray pulsar V 0332+53. Our model has profound implications for the interpretation of the data on the cyclotron lines observed in X-ray pulsars.

In order to predict the line parameters more accurately, a detailed model of the reflection of the column radiation from the atmosphere is required. It necessarily should include the dependence on the orientation of the local $B$-field as well as the angles of the incoming and reflected radiation. We would then be in a position to predict variations of the line energy and EW with the pulsar phase. This project is outside of the scope of the present paper and is left for a future study.

This research was supported by the Magnus Ehrnrooth foundation (AAM), the Academy of Finland (grant 127512, JP), the German Research Foundation (DFG) grant SFB/Transregio 7 "Gravitational Wave Astronomy" and the Russian Foundation for Basic Research (grants 12-02-97006-r-povolzhe-a, VFS; 11-02-01328 and 12-02-01265, AAL). We thank Alexander Serber for useful comments.

## APPENDIX

### A. EMISSION FROM THE RAPIDLY FALLING PLASMA IN AN ACCRETION COLUMN

Let us consider an accretion column with the gas falling with velocity $\beta = v/c$. Let us assume that the angular distribution of radiation escaping from the surface in the gas comoving frame is given by the bolometric intensity

$$I'(\zeta') = I_0\,(1 + a\cos\zeta'), \tag{A1}$$

where $\zeta'$ is the angle measured from the local normal to the surface, $I_0$ is a constant, and $a$ is the anisotropy parameter. In the calculations, we have chosen $a = 2$, which corresponds to the case of electron-scattering dominated optically thick atmosphere (Chandrasekhar 1960; Sobolev 1963), but keep here the formulae as general as possible. We define the coordinate system with the $z$-axis along the direction of motion of the gas, and the $x$-axis along the normal to the surface. The four-vector of the photon momentum in the lab frame is $\underline{k} = k\,\{1, \boldsymbol{\omega}\}$, where $k = h\nu/m_{\rm e}c^2$ and $\boldsymbol{\omega}$ is the unit vector along the photon momentum, which makes angle $\alpha$ with the $z$-axis: $\boldsymbol{\omega} = (\sin\alpha\cos\phi, \sin\alpha\sin\phi, \cos\alpha)$. Relative to the surface normal $\boldsymbol{n} = (1,0,0)$, it makes angle $\zeta$, so that $\cos\zeta = \boldsymbol{\omega}\cdot\boldsymbol{n} = \sin\alpha\cos\phi$.

The photon four-momentum in the frame comoving with the spot, $\underline{k'} = k'\,\{1, \boldsymbol{\omega'}\}$, is obtained from the Lorentz transformation. The energy is transformed as $k' = k/D$ and the unit vector along photon momentum is

$$\boldsymbol{\omega'} = \left( D\sin\alpha\cos\phi, D\sin\alpha\sin\phi, \frac{\cos\alpha - \beta}{1 - \beta\cos\alpha} \right). \tag{A2}$$

Here the Doppler factor is

$$D = \frac{1}{\gamma(1 - \beta\cos\alpha)}, \tag{A3}$$

and $\gamma = 1/\sqrt{1-\beta^2}$ is the Lorentz factor. Note that because of the relativistic aberration, the cosine of the projection angle we see the surface element that moves along its surface is (see also Poutanen & Gierliński 2003; Poutanen & Beloborodov 2006):

$$\cos\zeta' = D\cos\zeta = D\sin\alpha\cos\phi. \tag{A4}$$

The bolometric power emitted by a unit area surface element in the comoving frame per unit solid angle is given by

$$\frac{dL'}{d\boldsymbol{\omega}'} = I'(\zeta')\ \cos\zeta'. \tag{A5}$$

The angle-integrated emitted power is

$$L' = \oint \frac{dL'}{d\boldsymbol{\omega}'} d\boldsymbol{\omega}' = \int_0^{2\pi} d\varphi' \int_0^1 I'(\zeta')\ \cos\zeta'\, d\cos\zeta' = I_0\,\pi\left(1+\frac{2}{3}a\right). \tag{A6}$$

In order to evaluate the flux on the neutron star surface, we need to know the emitted power in the lab frame, which is given by (Rybicki & Lightman 1979)

$$\frac{dL}{d\boldsymbol{\omega}} = \frac{D^3}{\gamma}\frac{dL'}{d\boldsymbol{\omega}'} = \frac{D^4}{\gamma} I'(\zeta')\ \sin\alpha\cos\phi. \tag{A7}$$

Note that here the first transformation does not involve factor $D^4$, because we consider a steady-state source, not a moving blob (Rybicki & Lightman 1979; Sikora et al. 1997). For a thin accretion column, photons emitted at any azimuthal angles $\phi$ will have basically the same trajectory that is described just by angle $\alpha$. Thus, we can integrate over $\phi$ to obtain the final expression for the emission pattern

$$\frac{dL}{d\cos\alpha} = \int_{-\pi/2}^{\pi/2} d\phi\, \frac{dL}{d\omega} = I_0\,\frac{D^4}{\gamma}\ 2\ \sin\alpha\left(1 + a\,\frac{\pi}{4} D\sin\alpha\right). \tag{A8}$$

This expression is different somewhat from that given by Kaminker et al. (1976) and Mitrofanov & Tsygan (1978) as it contains one less Doppler factor. For the emission forward-back symmetric in the comoving frame, the total emitted power is Lorentz invariant (Rybicki & Lightman 1979), which can be checked by integrating expression (A8):

$$L = \int_{-1}^{1} \frac{dL}{d\cos\alpha} d\cos\alpha = L'. \tag{A9}$$

## B. PHOTON PROPAGATION IN THE VICINITY OF THE NEUTRON STAR

Figure 6 depicts the trajectory of a photon (red solid line) which is emitted at the accretion column at height $h$ above the neutron star surface in the direction that makes angle $\alpha$ with the radial direction towards the stellar center. The photon's path, described by the distance $r = R + h$ and azimuthal angle $\psi$, obeys the equation of motion (e.g. Misner et al. 1973; Pechenick et al. 1983):

$$\left(\frac{du}{d\psi}\right)^2 + (1-u)u^2 = \frac{1}{b^2}, \tag{B1}$$

where $u = r_{\rm S}/r$ and $b$ is the impact parameter in units of the Schwarzschild radius $r_{\rm S} = 2GM/c^2$ for a neutron star with mass $M$. The impact parameter and the angle, $\alpha$, between the radial direction and the photon trajectory are related by (e.g. Pechenick et al. 1983; Beloborodov 2002)

$$b = \frac{\sin\alpha}{u\sqrt{1-u}}. \tag{B2}$$

The azimuthal angle $\psi$ measured from the continuation of the trajectory towards infinity (dashed red line in Fig. 6) can be obtained from equation (B1):

$$\psi(r,\alpha) = \int_0^u du' \left[b^{-2} - (1-u')u'^2\right]^{-1/2}. \tag{B3}$$

For $r$ larger than $2r_{\rm S}$ the elliptic integral (B3) can be approximated with a high accuracy by (Beloborodov 2002; Poutanen & Beloborodov 2006)

$$\cos\alpha = u(r) + [1-u(r)]\cos\psi. \tag{B4}$$

The photon trajectory with impact parameter $b$ meets the neutron star surface of radius $R$ at an angle $\alpha_0$ relative to the normal, which is (see equation (B2)):

$$\sin\alpha_0 = \sin\alpha\ \frac{u(R)\sqrt{1-u(R)}}{u(r)\sqrt{1-u(r)}}. \tag{B5}$$

The intersection point lies at the azimuth $\psi_0$ that can be obtained from equation (B4) substituting there compactness $u = u(R) = r_{\rm S}/R$ and $\alpha_0$ instead of $\alpha$. Equation (B5) immediately constrains the maximum angle $\alpha$, when the trajectory is still intercepted by the star, corresponding to $\alpha_0 = \pi/2$:

$$\sin\alpha_{\rm max} = \frac{R}{r}\sqrt{\frac{1-u(r)}{1-u(R)}}. \tag{B6}$$

For a source at distance $r$ from the star emitting according to the angular pattern $dL(\alpha)/d\cos\alpha$ with total luminosity $L$, we then can obtain the fraction of radiation captured by the star:

$$\frac{L_{\rm c}}{L} = \frac{\int_{\cos\alpha_{\rm max}}^{1} \frac{dL(\alpha)}{d\cos\alpha}\ d\cos\alpha}{\int_{-1}^{1} \frac{dL(\alpha)}{d\cos\alpha}\ d\cos\alpha}. \tag{B7}$$

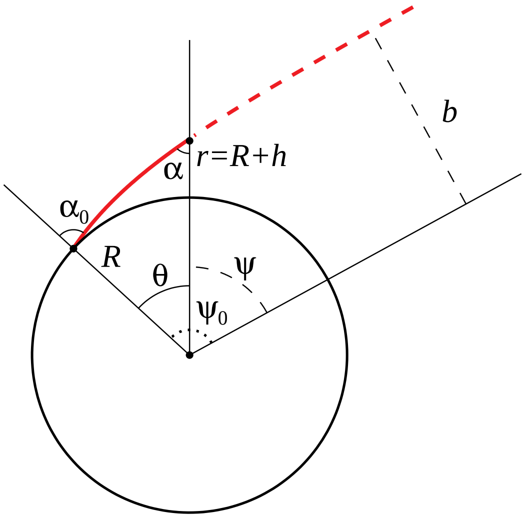

**Figure 6.** Geometry of light bending in Schwarzschild metric. The red solid line shows the photon trajectory from the emission point at distance $r = R + h$ to the stellar surface at radius $R$ and co-latitude $\theta$. The red dashed line is the continuation of the trajectory in the opposite direction to the infinity.

For an isotropic source, equation (B7) is reduced to

$$\frac{L_{\rm c}}{L} = \frac{1}{2}\left(1 - \cos\alpha_{\max}\right). \tag{B8}$$

Distribution of the intercepted luminosity over the neutron star surface is given by

$$\frac{dL_{\rm c}(\theta)}{d\cos\theta} = \frac{dL(\alpha)}{d\cos\alpha}\,\frac{d\cos\alpha}{d\cos\theta}\,\frac{dL_{\rm c}}{dL}, \tag{B9}$$

where the first factor on the rhs is the specified emission pattern. We compute the second factor numerically differentiating $\theta = \psi_0 - \psi$ as a function of $\alpha$, with both $\psi$ and $\psi_0$ obtained via approximate light bending equation (B4) and $\alpha_0$ from equation (B5). The last factor, $dL_{\rm c}/dL = [1 - u(r)]/[1 - u(R)]$, just contains two redshift factors of the type $1 + z = 1/\sqrt{1-u}$: one from the photon energy change in the gravitational field and another one from the time dilation.

## REFERENCES

Araya, R. A. & Harding, A. K. 1999, ApJ, 517, 334
Araya-Góchez, R. A. & Harding, A. K. 2000, ApJ, 544, 1067
Avrett, E. H. 1965, SAO Special Report, 174, 101
Avrett, E. H. & Hummer, D. G. 1965, MNRAS, 130, 295
Basko, M. M. & Sunyaev, R. A. 1976, MNRAS, 175, 395
Beloborodov, A. M. 2002, ApJ, 566, L85
Burderi, L., Di Salvo, T., Robba, N. R., La Barbera, A., & Guainazzi, M. 2000, ApJ, 530, 429
Caballero, I., et al. 2013, ApJ, 764, L23
Caballero, I. & Wilms, J. 2012, Mem. Soc. Astron. Italiana, 83, 230
Chandrasekhar, S. 1960, Radiative transfer (New York: Dover)
Coburn, W., Heindl, W. A., Rothschild, R. E., et al. 2002, ApJ, 580, 394
Filippova, E. V., Tsygankov, S. S., Lutovinov, A. A., & Sunyaev, R. A. 2005, Astron. Lett., 31, 729
Harding, A. K. & Lai, D. 2006, Reports on Progress in Physics, 69, 2631
Ivanov, V. V. 1973, Transfer of radiation in spectral lines (Washington: US Department of Commerce, National Bureau of Standards)
Kaminker, A. D., Fedorenko, V. N., & Tsygan, A. I. 1976, Soviet Ast., 20, 436
Klochkov, D., et al. 2012, A&A, 542, L28
Kreykenbohm, I., et al. 2008, A&A, 492, 511
Lyubarskii, Y. E. & Sunyaev, R. A. 1988, Soviet Astronomy Letters, 14, 390
Mihara, T., Makishima, K., & Nagase, F. 1998, Adv. Sp. Res., 22, 987
Misner, C. W., Thorne, K. S., & Wheeler, J. A. 1973, Gravitation (San Francisco: W.H. Freeman and Co.)
Mitrofanov, I. G. & Tsygan, A. I. 1978, A&A, 70, 133
Pavlov, G. G., Mitrofanov, I. G., & Shibanov, I. A. 1980, Ap&SS, 73, 63
Pechenick, K. R., Ftaclas, C., & Cohen, J. M. 1983, ApJ, 274, 846
Poutanen, J. & Beloborodov, A. M. 2006, MNRAS, 373, 836
Poutanen, J. & Gierliński, M. 2003, MNRAS, 343, 1301
Rybicki, G. B. & Lightman, A. P. 1979, Radiative processes in astrophysics (New York: Wiley-Interscience)

Sikora, M., Madejski, G., Moderski, R., & Poutanen, J. 1997, ApJ, 484, 108
Sobolev, V. V. 1963, A treatise on radiative transfer (Princeton: Van Nostrand)
Staubert, R., Shakura, N. I., Postnov, K., et al. 2007, A&A, 465, L25
Suleimanov, V., Poutanen, J., Revnivtsev, M., & Werner, K. 2011, ApJ, 742, 122
Suleimanov, V. F., Pavlov, G. G., & Werner, K. 2012, ApJ, 751, 15
Tsygankov, S. S., Lutovinov, A. A., Churazov, E. M., & Sunyaev, R. A. 2006, MNRAS, 371, 19
Tsygankov, S. S., Lutovinov, A. A., & Serber, A. V. 2010, MNRAS, 401, 1628
Wasserman, I. & Salpeter, E. 1980, ApJ, 241, 1107